PERGAMON

International Journal of Solids and Structures 38 (2001) 4721–4740

INTERNATIONAL JOURNAL OF SOLIDS and STRUCTURES

www.elsevier.com/locate/ijsolstr

The electromechanical behavior of a piezoelectric actuator bonded to an anisotropic elastic medium

X.D. Wang *, G.L. Huang

Department of Mechanical Engineering, University of Alberta, 4–9 Mechanical Engineering Building, Edmonton, Al., Canada T6G 2G8

Received 18 April 2000; in revised form 7 June 2000

Abstract

Significant efforts have been made in the study of electromechanical behavior of piezoelectric structures. However, the success has been mainly confined to the global response of the structures. This paper provides a comprehensive analytical study on the load transfer between a piezoceramic actuator and an anisotropic elastic medium under in-plane mechanical and electrical loading. The actuator is characterized by an electroelastic line model with the poling direction being perpendicular to its length. The electrically induced local stress field is studied in detail by using Fourier transform technique and solving the resulting integral equations in terms of the interfacial shear stress. Typical examples are provided to show the effects of the geometry, the material combination and the material anisotropy of the composite on the load transfer. The study is further extended to treat the interfacial debonding between the actuator and the host material. The load transfer predicted by the current model is found to be in good quantitative accord with the FEM analysis for general orthotropic structures.

Keywords: Piezoelectric actuator; Smart structures; Anisotropy; Load transfer; Singularity; Debonding

1. Introduction

The emergence of new piezoceramic materials, which are capable of generating larger strains under electric fields, had revived the intense research and development of new piezoceramic actuators for structural applications. Piezoceramic materials have the advantages of quick response, low power consumption and high linearity. As a result, they had been used in the design of different advanced structures, e.g. large-scale space structures, aircraft structures, satellites, etc. In addition, piezoceramic actuators can be easily fabricated into different desired shapes which can be used in different applications to achieve the highest possible displacement or force for the lowest possible voltage. It is possible now to integrate piezoceramic actuators with conventional structural materials to serve as energy input devices or actuating elements in many engineering applications (Ashley, 1995; Dosch et al., 1995; Gandhi and Thompson, 1992; Ha et al., 1992; Varadan et al., 1993).

* Corresponding author. Fax: +1-780-492-2200.
E-mail address: xiaodong.wang@ualberta.ca (X.D. Wang).

0020-7683/01/$ - see front matter
PII: S0020-7683(00)00299-7

One of the most fundamental issues surrounding the effectiveness of a piezoelectric actuator in a smart structure system is to determine the actuation effect being transferred from the actuator to the host structure, which necessitates the accurate assessment of the local stress distribution around the actuator.

Crawley and de Luis (1987) first analyzed a beam-like structure with surface bonded and embedded thin sheet piezoelectric actuators to study the load transfer between the actuator and the host beam. In that analysis, the axial stress in the actuator was assumed to be uniform across its thickness, and the host structure was treated as a Bernoulli–Euler beam. This model was further modified using a Bernoulli–Euler model of a piezoelectric actuator by considering the linear stress distribution along its thickness (Crawley and Anderson, 1990). Im and Atluri (1989) further modified the actuator model presented by Crawley and de Luis (1987) by considering both the axial and the transverse shear forces in the beam. A refined actuator model based on the plane stress condition was presented for a beam structure with symmetrically surface-bonded actuator patches (Lin and Rogers, 1993a,b).

Plate and shell models have been extensively used in modeling piezoelectric structures. Wang and Rogers (1991) modified the classical laminated plate theory to model actuator-induced bending and extension of laminated plates under static loading. Tauchert (1992) further investigated the control of thermal deformation of laminated plates using piezoelectric actuators. Typical examples also include the work by Dimitriadis et al. (1991), Tzou and Tseng (1991), Mitchell and Reddy (1995), Bank and Smith (1995), Reddy (1997), Han and Lee (1998) and Reddy (1999). Finite element method is currently also being used for active vibration and noise control of piezoelectric structures (Tzou and Ye, 1994; Lim et al., 1999).

In spite of the fact that different methods have been developed to treat piezoelectric structures, existing work is mainly focused on the global response of these systems. Because of the difficulties associated with the complicated electromechanical coupling, material inhomogeneity and anisotropy, solutions representing the local electromechanical behavior around piezoelectric actuators have not been properly established. Recently, Wang and Meguid (2000) studied the load transfer between a thin piezoelectric actuator and an isotropic host medium. The singular stress field around the actuator tip was studied.

This article is concerned with the development of an analytical solution to describe coupled electromechanical behavior of a piezoceramic actuator bonded to an infinite orthotropic elastic medium under in-plane mechanical and electrical loads. The actuator was characterized using a one-dimensional model. The load transfer between a piezoelectric actuator and the host structure was determined by using Fourier transform technique and solving the resulting integral equations in terms of the interfacial shear stress. The analytical expression of the local stress field around the actuator was studied in detail. Specifically, two aspects of the work were examined. The first was concerned with determining the effect of the geometry, the material mismatch and the material anisotropy on the load transfer between the actuator and the host structure, while the second was concerned with the effect of interfacial debonding.

2. Formulation of the problem

Consider now the plane strain problem of a thin piezoceramic actuator bonded to a homogeneous orthotropic elastic medium, as illustrated in Fig. 1. The poling direction of the actuator is along the z-axis, and the halflength and the thickness of the actuator are denoted by c and h, respectively. An electric field E_z is applied along the poling direction of the actuator by applying a voltage (ΔV) between the upper and the lower electrodes of the actuator, with $E_z = -\Delta V/h$.

For a thin actuator, for which the thickness is very small compared to its length, the applied electric field will mainly result in an axial deformation. The axial stress and displacement can then be assumed to be uniform across the thickness of the actuator, and the interfacial shear stress (τ) transferred between the actuator and the host can be replaced by a distributed body force along the actuator. Accordingly, the actuator can be modeled as an electroelastic line subjected to the applied electric field and the distributed

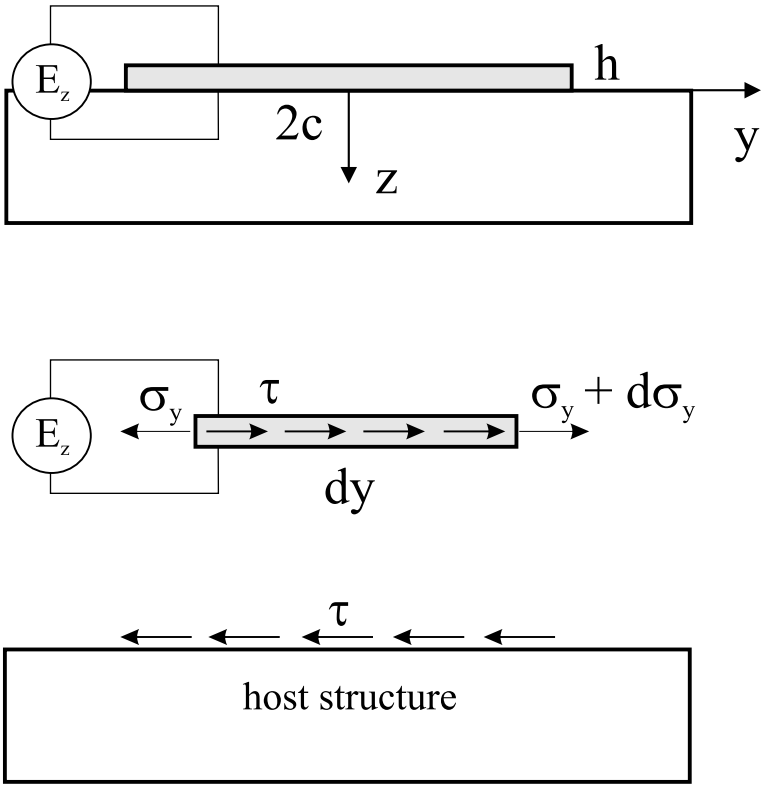

Fig. 1. Actuator model.

axial force, τ/h, as shown in Fig. 1. By using the equilibrium condition and the traction-free conditions at the ends of the actuator, the axial stress in the actuator can be expressed in terms of the shear stress τ as

$$\sigma_y(y) = -\int_{-c}^{y} \frac{\tau(\xi)}{h}\,\mathrm{d}\xi \tag{1}$$

with

$$\int_{-c}^{c} \tau(\xi)\,\mathrm{d}\xi = 0. \tag{2}$$

The relation between the stress, the strain and the electric field of this actuator can be obtained by using the following general constitutive relation:

$$\sigma_y = E_\mathrm{a}\epsilon_y - e_\mathrm{a}E_z, \tag{3}$$

where E_a and e_a are effective material constants given in Appendix A. The resulting axial strain can then be expressed in terms of τ as

$$\epsilon_y(y) = -\frac{1}{E_\mathrm{a}h}\int_{-c}^{y} \tau(\xi)\,\mathrm{d}\xi + \frac{e_\mathrm{a}}{E_\mathrm{a}}E_z, \quad |y| < c. \tag{4}$$

Consider now the deformation of the host orthotropic elastic medium with the principal elastic axes being parallel to the y and z axes. The solution of the displacement components can be obtained by solving

the governing equations of the problem using Fourier transform technique, as shown in Appendix B. The general solution in Fourier transform domain can be expressed as

$$\overline{v} = \begin{cases} G_1^+ \mathrm{e}^{-z_1} + H_1^+ \mathrm{e}^{-z_2}, & c_{33} < \frac{1}{2}(\sqrt{c_{11}c_{22}} - c_{12}), \\ (G_1 + H_1 z_0)\mathrm{e}^{-z_0}, & c_{33} = \frac{1}{2}(\sqrt{c_{11}c_{22}} - c_{12}), \\ G_1^- \mathrm{e}^{-z_3}\cos z_4 + H_1^- \mathrm{e}^{-z_3}\sin z_4, & c_{33} > \frac{1}{2}(\sqrt{c_{11}c_{22}} - c_{12}), \end{cases} \tag{5}$$

and

$$\overline{w} = \frac{1}{c_{33}s^2}\left[\frac{c_{22}c_{33}}{\mathrm{i}s(c_{12}+c_{33})}\frac{\partial^3 \overline{v}}{\partial z^3} + \frac{\mathrm{i}s\left[c_{11}c_{22} - (c_{12}+c_{33})^2\right]}{c_{12}+c_{33}}\frac{\partial \overline{v}}{\partial z}\right], \tag{6}$$

where c_{ij} are elastic constants of the medium, and $\overline{v}$, $\overline{w}$ are Fourier transform of the displacement components in the y and z directions, respectively. It should be noted that an isotropic medium will satisfy the relation $c_{33} = (1/2)(\sqrt{c_{11}c_{22}} - c_{12})$. In the above equations,

$$z_0 = \beta_0|s|z, \quad z_1 = \beta_1|s|z, \quad z_2 = \beta_2|s|z, \quad z_3 = \beta_3|s|z, \quad z_4 = \beta_4|s|z,$$

$$\beta_0 = \sqrt{u_1}, \quad \beta_1 = \sqrt{u_1 + \sqrt{u_1^2 - u_2}}, \quad \beta_2 = \sqrt{u_1 - \sqrt{u_1^2 - u_2}},$$

$$\beta_3 = \sqrt{\frac{\sqrt{u_2} + u_1}{2}}, \qquad \beta_4 = \sqrt{\frac{\sqrt{u_2} - u_1}{2}},$$

$$u_1 = \frac{c_{11}c_{22} + c_{33}^2 - (c_{12}+c_{33})^2}{2c_{22}c_{33}}, \qquad u_2 = \frac{c_{11}}{c_{22}},$$

and G_1^+, H_1^+, G_1, H_1, G_1^-, H_1^- are functions of s to be determined from the boundary conditions of the problems.

The halfspace will be deformed by the piezoelectric actuator through an interfacial shear stress at $z = 0$, which can be expressed as

$$\tau_{yz} = \begin{cases} -\tau(y), & |y| < c, \\ 0, & \text{otherwise.} \end{cases} \tag{7}$$

Using this boundary condition, the unknown functions in Eqs. (5) and (6) can be determined, and the resulting strain along $z = 0$ can be expressed as

$$\epsilon_y(y,0)|_{\text{host}} = \frac{2}{\pi \overline{\overline{E}}}\int_{-c}^{c} \frac{\tau(\xi)}{y-\xi}\,\mathrm{d}\xi, \tag{8}$$

where $\overline{E}$ is an effective elastic modulus of the host medium given by

$$\overline{E} = \begin{cases} \dfrac{2K_1K_2(\beta_2 - \beta_1)}{(K_1+K_2)(c_{12}+c_{33})}, & c_{33} < \frac{1}{2}(\sqrt{c_{11}c_{22}} - c_{12}), \\ \dfrac{2\overline{K}_2^2}{\overline{\overline{K}}_1(c_{12}+c_{33})}, & c_{33} = \frac{1}{2}(\sqrt{c_{11}c_{22}} - c_{12}), \\ \dfrac{2\beta_4(\overline{\overline{K}}_1^2 + \overline{\overline{K}}_2^2)}{\overline{\overline{K}}_1(c_{12}+c_{33})}, & c_{33} > \frac{1}{2}(\sqrt{c_{11}c_{22}} - c_{12}), \end{cases} \tag{9}$$

where

$$K_1 = -(c_{22}c_{33}\beta_2^2 - c_{11}c_{22} + c_{12}^2 + c_{12}c_{33}), \quad K_2 = (c_{22}c_{33}\beta_1^2 - c_{11}c_{22} + c_{12}^2 + c_{12}c_{33}),$$
$$\overline{K}_1 = 2c_{22}c_{33}\beta_0^2, \quad \overline{K}_2 = c_{22}c_{33}\beta_0^2 - c_{11}c_{22} + c_{12}^2 + c_{12}c_{33},$$
$$\overline{\overline{K}}_1 = 2\beta_3\beta_4 c_{22}c_{33}, \quad \overline{\overline{K}}_2 = c_{22}c_{33}(\beta_3^2 - \beta_4^2) - c_{11}c_{22} + c_{12}^2 + c_{12}c_{13}.$$

For the case where the shear modulus c_{33} is very small, $c_{33} \to 0$, $\overline{E}$ tends to zero. For the case where $c_{33} \to \infty$, $\overline{E}$ tends to infinity. An isotropic host medium, which corresponds to $c_{33} = (c_{11} - c_{12})/2$ will result in $\overline{E} = E/(1 - \nu^2)$ with E and ν being Young's modulus and the Poisson ratio, respectively.

The compatibility of deformation between the actuator and the host structure indicates that

$$\epsilon_y|_{\text{actuator}} = \epsilon_y|_{\text{host}}, \qquad |y| < c, \quad z = 0. \tag{10}$$

Substituting Eqs. (4) and (8) into Eq. (10) gives

$$\frac{2}{\pi\overline{\overline{E}}}\int_{-c}^{c}\frac{\tau(\xi)}{y-\xi}\mathrm{d}\xi + \frac{1}{hE_{\mathrm{a}}}\int_{c}^{y}\tau(\xi)\,\mathrm{d}\xi = \frac{e_{\mathrm{a}}E_z}{E_{\mathrm{a}}}, \quad |y| < c. \tag{11}$$

Eq. (11) can be used to determine interfacial shear stress τ. It is interesting to note that, based on the current actuator model, the elastic property of the orthotropic host structure is governed by only one parameter $\overline{E}$. The suitability of using $\overline{E}$ to represent the behavior of general orthotropic host media will be discussed in detail in Section 5.

The singular integral equation (11) and Eq. (2) can be normalized to give

$$\begin{aligned}&\int_{-1}^{1}\frac{\overline{\tau}(\zeta)\,\mathrm{d}\zeta}{\eta-\zeta} + q\alpha\int_{-1}^{\eta}\overline{\tau}(\zeta)\,\mathrm{d}\zeta = q, \quad |\eta| < 1,\\ &\int_{-1}^{1}\overline{\tau}(\zeta)\,\mathrm{d}\zeta = 0,\end{aligned} \tag{12}$$

where

$$\begin{aligned}&\overline{\tau}(\eta) = \tau(c\eta)/\sigma_B, \quad \eta = y/c,\\ &q = \frac{\pi\overline{E}}{2E_{\mathrm{a}}}, \qquad \sigma_B = e_{\mathrm{a}}E_z, \qquad \alpha = c/h.\end{aligned} \tag{13}$$

Since Eq. (12) is a singular integral equation of the first kind, the solution of it involves a square-root singularity (Muskhelishvili, 1953) at $|\eta| = 1$. Accordingly, the solution of Eq. (12) can be generally expressed in terms of the first kind of Chebyshev polynomials, T_j, as

$$\overline{\tau}(\eta) = \frac{1}{\sqrt{1-\eta^2}}\sum_{j=1}^{\infty} d_j T_j(\eta). \tag{14}$$

By truncating the Chebyshev polynomial expansion to the Nth term and satisfying the integral equation in expression (12) at the following collocation points along the actuator,

$$\eta_k = \cos\frac{k-1}{N-1}\pi, \quad k = 1, 2, \ldots, N, \tag{15}$$

and the unknown coefficients d_j can be determined by solving the following algebraic equations

$$\sum_{j=1}^{N} d_j \frac{\sin\left(j\dfrac{k-1}{N-1}\pi\right)}{\sin\left(\dfrac{k-1}{N-1}\pi\right)}\left[1 + \frac{q\alpha}{\pi j}\sin\left(\frac{k-1}{N-1}\pi\right)\right] = -q/\pi, \quad k = 1, 2, \ldots, N. \tag{16}$$

The interfacial shear stress can then be determined using Eq. (16). The singular behavior of the interfacial shear stress at the right tip of the actuator is characterized by the following shear stress singularity factor (SSSF) S:

$$S = \lim_{y\to c}\left[\sqrt{2\pi(c-y)}\tau(y)\right] = \sigma_B\sqrt{c\pi}\sum_{j=1}^{N} d_j. \tag{17}$$

3. Load transfer and stress distribution

The most important issue in actuator design is the load transfer from the actuator to the host structure. Using the current actuator model, the electrically induced stress field in the host medium can be obtained analytically. According to the general solution given by Eqs. (5) and (6), the stress distribution in the host medium can be obtained in terms of interfacial shear stress τ.

For the case where $c_{33} < (\sqrt{c_{11}c_{22}} - c_{12})/2$, the induced stress field is

$$\sigma_y = \frac{1}{\pi}\int_{-c}^{c}\int_{0}^{\infty}\left[K_3\,\mathrm{e}^{-\beta_1 sz} + K_4\,\mathrm{e}^{-\beta_2 sz}\right]\sin[s(u-y)]\tau(0,u)\,\mathrm{d}s\,\mathrm{d}u, \tag{18}$$

$$\sigma_z = \frac{1}{\pi}\int_{-c}^{c}\int_{0}^{\infty}\left[K_5\,\mathrm{e}^{-\beta_1 sz} + K_6\,\mathrm{e}^{-\beta_2 sz}\right]\sin[s(u-y)]\tau(0,u)\,\mathrm{d}s\,\mathrm{d}u, \tag{19}$$

$$\sigma_{yz} = \frac{1}{\pi}\int_{-c}^{c}\int_{0}^{\infty}\left[K_7\,\mathrm{e}^{-\beta_1 sz} + K_8\,\mathrm{e}^{-\beta_2 sz}\right]\cos[s(u-y)]\tau(0,u)\,\mathrm{d}s\,\mathrm{d}u, \tag{20}$$

where K_3, K_4, K_5, K_6, K_7 and K_8 are defined in Appendix C. Using the solution of τ given by Eq. (14), the integration in Eqs. (18)–(20) can be completed, and these stress components can be expressed in explicit forms as

$$\sigma_y = \sum_{j=1}^{\infty} d_j\begin{cases}(-1)^n\left[K_3F_{1j}(\phi_1,\theta_1) + K_4F_{1j}(\phi_2,\theta_2)\right], & j = 2n+1,\\ (-1)^n\left[K_3F_{2j}(\phi_1,\theta_1) + K_4F_{2j}(\phi_2,\theta_2)\right], & j = 2n,\end{cases} \tag{21}$$

$$\sigma_z = \sum_{j=1}^{\infty} d_j\begin{cases}(-1)^n\left[K_5F_{1j}(\phi_1,\theta_1) + K_6F_{1j}(\phi_2,\theta_2)\right], & j = 2n+1,\\ (-1)^n\left[K_5F_{2j}(\phi_1,\theta_1) + K_6F_{2j}(\phi_2,\theta_2)\right], & j = 2n,\end{cases} \tag{22}$$

$$\sigma_{yz} = \sum_{j=1}^{\infty} d_j\begin{cases}(-1)^n\left[K_7F_{1j}(\phi_1,\theta_1) + K_8F_{1j}(\phi_2,\theta_2)\right], & j = 2n,\\ (-1)^{n+1}\left[K_7F_{2j}(\phi_1,\theta_1) + K_8F_{2j}(\phi_2,\theta_2)\right], & j = 2n+1,\end{cases} \tag{23}$$

where F_{1j}, F_{2j} are known functions and ϕ_1, ϕ_2, θ_1, θ_2 are functions of y and z, as given in Appendix C.

For $c_{33} = (\sqrt{c_{11}c_{22}} - c_{12})/2$,

$$\sigma_y = \sum_{j=1}^{\infty} d_j\begin{cases}(-1)^n\left[\overline{K}_3F_{1j}(\phi_0,\theta_0) - z\overline{K}_4\frac{\partial}{\partial z}F_{1j}(\phi_0,\theta_0)\right], & j = 2n+1,\\ (-1)^n\left[\overline{K}_3F_{2j}(\phi_0,\theta_0) - z\overline{K}_4\frac{\partial}{\partial z}F_{2j}(\phi_0,\theta_0)\right], & j = 2n,\end{cases} \tag{24}$$

$$\sigma_z = \sum_{j=1}^{\infty} d_j\begin{cases}(-1)^{n+1}\left[z\overline{K}_6\frac{\partial}{\partial z}F_{1j}(\phi_0,\theta_0)\right], & j = 2n+1,\\ (-1)^{n+1}\left[z\overline{K}_6\frac{\partial}{\partial z}F_{2j}(\phi_0,\theta_0)\right], & j = 2n,\end{cases} \tag{25}$$

$$\sigma_{yz} = \sum_{j=1}^{\infty} d_j \begin{cases} (-1)^n \left[\overline{K}_7 F_{1j}(\phi_0, \theta_0) - z\overline{K}_8 \frac{\partial}{\partial z} F_{1j}(\phi_0, \theta_0)\right], & j = 2n, \\ (-1)^{n+1} \left[\overline{K}_7 F_{2j}(\phi_0, \theta_0) - z\overline{K}_8 \frac{\partial}{\partial z} F_{2j}(\phi_0, \theta_0)\right], & j = 2n+1, \end{cases} \tag{26}$$

where $\overline{K}_3$, $\overline{K}_4$, $\overline{K}_6$, $\overline{K}_7$ and $\overline{K}_8$ depended only on material constants and ϕ_0, θ_0 are functions of y and z, as given in Appendix C.

For $c_{33} > (\sqrt{c_{11}c_{22}} - c_{12})/2$,

$$\sigma_y = \sum_{j=1}^{\infty} d_j \begin{cases} (-1)^n \left[\overline{\overline{K}}_3 F_{3j}(\phi_3, \theta_3, \phi_4, \theta_4) + \overline{\overline{K}}_4 F_{4j}(\phi_3, \theta_3, \phi_4, \theta_4)\right], & j = 2n+1, \\ (-1)^n \left[\overline{\overline{K}}_3 F_{5j}(\phi_3, \theta_3, \phi_4, \theta_4) + \overline{\overline{K}}_4 F_{6j}(\phi_3, \theta_3, \phi_4, \theta_4)\right], & j = 2n, \end{cases} \tag{27}$$

$$\sigma_z = \sum_{j=1}^{\infty} d_j \begin{cases} (-1)^n \left[\overline{\overline{K}}_5 F_{3j}(\phi_3, \theta_3, \phi_4, \theta_4) + \overline{\overline{K}}_6 F_{4j}(\phi_3, \theta_3, \phi_4, \theta_4)\right], & j = 2n+1, \\ (-1)^n \left[\overline{\overline{K}}_5 F_{5j}(\phi_3, \theta_3, \phi_4, \theta_4) + \overline{\overline{K}}_6 F_{6j}(\phi_3, \theta_3, \phi_4, \theta_4)\right], & j = 2n, \end{cases} \tag{28}$$

$$\sigma_{yz} = \sum_{j=1}^{\infty} d_j \begin{cases} (-1)^{n+1} \left[\overline{\overline{K}}_7 F_{3j}(\phi_3, \theta_3, \phi_4, \theta_4) + \overline{\overline{K}}_8 F_{4j}(\phi_3, \theta_3, \phi_4, \theta_4)\right], & j = 2n+1, \\ (-1)^n \left[\overline{\overline{K}}_7 F_{5j}(\phi_3, \theta_3, \phi_4, \theta_4) + \overline{\overline{K}}_8 F_{6j}(\phi_3, \theta_3, \phi_4, \theta_4)\right], & j = 2n, \end{cases} \tag{29}$$

where $\overline{\overline{K}}_3$, $\overline{\overline{K}}_4$, $\overline{\overline{K}}_5$, $\overline{\overline{K}}_6$, $\overline{\overline{K}}_7$, $\overline{\overline{K}}_8$ are material constants, F_{3j} and F_{4j} are known functions and ϕ_3, θ_3, ϕ_4, θ_4 are functions of y and z, as given in Appendix C.

4. Interfacial debonding

Local stress concentration and/or weak interfacial bonding may result in partial debonding between the actuator and the host material. The debonding will result in further stress concentration and change the load transfer. To simulate this situation, the actuator considered is assumed symmetrically debonded in $|y| < d$, as shown in Fig. 2.

By making use of the equilibrium equation (1) and the traction-free condition at the two ends of the actuator, the resulting axial strain can be expressed in terms of τ as

$$\epsilon_y(y)|_{\text{actuator}} = \begin{cases} \dfrac{\sigma_d + e_a E_z}{E_a}, & 0 < y < d, \\ \dfrac{1}{E_a h}\left[\sigma_d h - \displaystyle\int_d^y \tau(\xi)\,\mathrm{d}\xi\right] + \dfrac{e_a}{E_a} E_z, & d < y < c, \end{cases} \tag{30}$$

where

$$\sigma_d = \int_d^c \frac{\tau(\xi)}{h}\,\mathrm{d}\xi \tag{31}$$

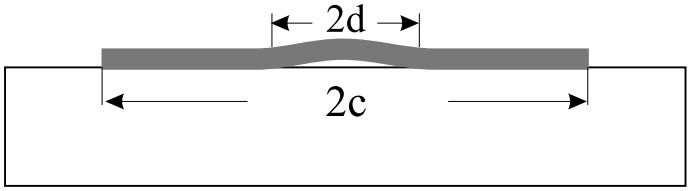

Fig. 2. A debonded actuator.

is the axial stress in the debonded part of the actuator.

Similar to the case where the actuator is perfectly bonded, the strain along $z = 0$ in the host material can be expressed in terms of τ:

$$\epsilon_y(y,0)|_{\text{host}} = \frac{2}{\pi\bar{E}}\left[\int_d^c \tau(\xi)\left(\frac{1}{y-\xi}-\frac{1}{y+\xi}\right)\mathrm{d}\xi\right]. \tag{32}$$

The continuity between the actuator and the host structure indicates that

$$\epsilon_y|_{\text{actuator}} = \epsilon_y|_{\text{host}}, \qquad d < y < c, \quad z = 0 \tag{33}$$

and

$$u_y(d)|_{\text{actuator}} - u_y(0)|_{\text{actuator}} = u_y(d,0)|_{\text{host}} - u_y(0,0)|_{\text{host}}. \tag{34}$$

Substituting Eqs. (30) and (32) into Eqs. (33) and (34), the following normalized equations can be obtained as

$$\int_{-1}^{1}\frac{\overline{\tau}(\zeta)\,\mathrm{d}\zeta}{\eta-\zeta} - \int_{-1}^{1}\frac{\overline{\tau}(\zeta)\,\mathrm{d}\zeta}{2(1+\alpha-2\alpha_1)+\eta+\zeta} - q\alpha_1\int_{\eta}^{l}\overline{\tau}(\zeta)\,\mathrm{d}\zeta = q, \quad |\eta|<1, \tag{35}$$

$$\alpha_1\int_{\eta^*}^{-1}\int_{-1}^{1}\frac{\overline{\tau}(\zeta)\,\mathrm{d}\zeta}{\eta-\zeta}\mathrm{d}\eta = q(\alpha-2\alpha_1)(\sigma^*+1), \tag{36}$$

with

$$\int_{-1}^{1}\overline{\tau}(\zeta)\,\mathrm{d}\zeta = \frac{\sigma^*}{\alpha_1}. \tag{37}$$

The normalized stresses are given by

$$\overline{\tau}(\zeta) = \tau(c_1\zeta + y^*)/\sigma_B, \qquad \sigma^* = \sigma_d/\sigma_B \tag{38}$$

with

$$\begin{aligned} &\eta = (y-y^*)/c_1, \qquad \alpha = c/h, \qquad \alpha_1 = c_1/h,\\ &c_1 = \frac{1}{2}(c-d), \qquad y^* = \frac{1}{2}(c+d), \qquad \eta^* = 3-2\frac{\alpha}{\alpha_1}. \end{aligned} \tag{39}$$

The general solutions of τ can then be expressed in terms of the following Chebyshev polynomials,

$$\overline{\tau}(\eta) = \frac{1}{\sqrt{1-\eta^2}}\sum_{j=0}^{\infty} d_j T_j(\eta), \tag{40}$$

where $d_0 = \sigma^*/(\pi q\alpha_1)$ to satisfy Eq. (37).

If the Chebyshev polynomial expansion is truncated to the Nth term, and Eq. (35) is satisfied at the following collocation points along the bonded segment of the actuator given by

$$\eta_k = \cos\frac{k-1}{N-1}\pi, \quad k = 1,2,\ldots,N, \tag{41}$$

Eq. (35) reduces to

$$\sum_{j=1}^{N} d_j \frac{\sin\left(j\frac{k-1}{N-1}\pi\right)}{\sin\left(\frac{k-1}{N-1}\pi\right)}\left[1+\frac{q\alpha_1}{\pi j}\sin\left(\frac{k-1}{N-1}\pi\right)\right]+\sum_{j=1}^{N} d_j\left[\left(\eta_k^2-1\right)^{1/2}+\eta_k\right]^j\Big/\sqrt{\eta_k^2-1}$$
$$+\frac{\sigma^*}{\pi}\left\{\frac{1}{\alpha_1\sqrt{\eta_k^2-1}}+q\frac{k-1}{N-1}\right\}=-q/\pi,\quad k=1,2,\ldots,N. \tag{42}$$

In addition, Eq. (36) becomes

$$\sigma^*\left\{-\ln\left[\left|-\eta^*+\sqrt{\eta^{*2}-1}\right|\Big/\left|\eta^*+\sqrt{\eta^{*2}-1}\right|\right]-2(\alpha-2\alpha_1)q\right\}+2$$
$$\times\sum_{j=1}^{N} d_j\left\{-\pi\alpha_1\int_{\eta^*}^{-1}\left[\left(\eta^2-1\right)^{1/2}+\eta\right]^j\Big/\sqrt{\eta^2-1}\,\mathrm{d}\eta\right\}=2(\alpha-2\alpha_1). \tag{43}$$

From these equations, the unknown coefficient d_j can be determined. The resulting SSSF at the right end of the debonding part can be obtained as

$$S=\sigma_B\sqrt{c_1\pi}\sum_{j=0}^{N}(-1)^j d_j. \tag{44}$$

5. Analysis and discussion

5.1. Effective modulus $\overline{E}$

One of the most important parameters governing the load transfer between the actuator and the host material is the effective modulus of the host medium $\overline{E}$ given by Eq. (9). Fig. 3 shows the effect of material anisotropy of the host medium upon the normalized effective modulus $E^*=\overline{E}/c_{11}$ for $c_{12}/c_{11}=0.15$. It is observed that the effective modulus $\overline{E}$ is very sensitive to the shear modulus c_{33}. For cases where c_{22}/c_{11} is small (<0.3 for example), c_{22} shows a significant effect upon $\overline{E}$, which corresponds to the case where $c_{33}>(1/2)\left(\sqrt{c_{11}c_{22}}-c_{12}\right)$. In comparison, Fig. 4 shows the effect of the Poisson ratio $v_{yz}=c_{12}/c_{11}$ upon $\overline{E}$ for $c_{33}/c_{11}=0.1$. It is interesting to note that the effective modulus is relatively insensitive to the change of the Poisson ratio for $c_{22}/c_{11}>0.5$.

5.2. Singular stress field around the actuator

The singular stress field near the tip of the actuator can be obtained by using the substitution that

$$y=c+r\cos\theta,\qquad z=r\sin\theta \tag{45}$$

and considering the asymptotic property of Eqs. (21)–(29) when $r\to 0$.

For $c_{33}<(\sqrt{c_{11}c_{22}}-c_{12})/2$, the singular stress field is given by

$$\sigma_y=S\frac{[K_3 f_1(\beta_1,\theta_1)+K_4 f_1(\beta_2,\theta_2)]}{\sqrt{r\pi}}, \tag{46}$$

$$\sigma_z=S\frac{[K_5 f_1(\beta_1,\theta_1)+K_6 f_1(\beta_2,\theta_2)]}{\sqrt{r\pi}}, \tag{47}$$

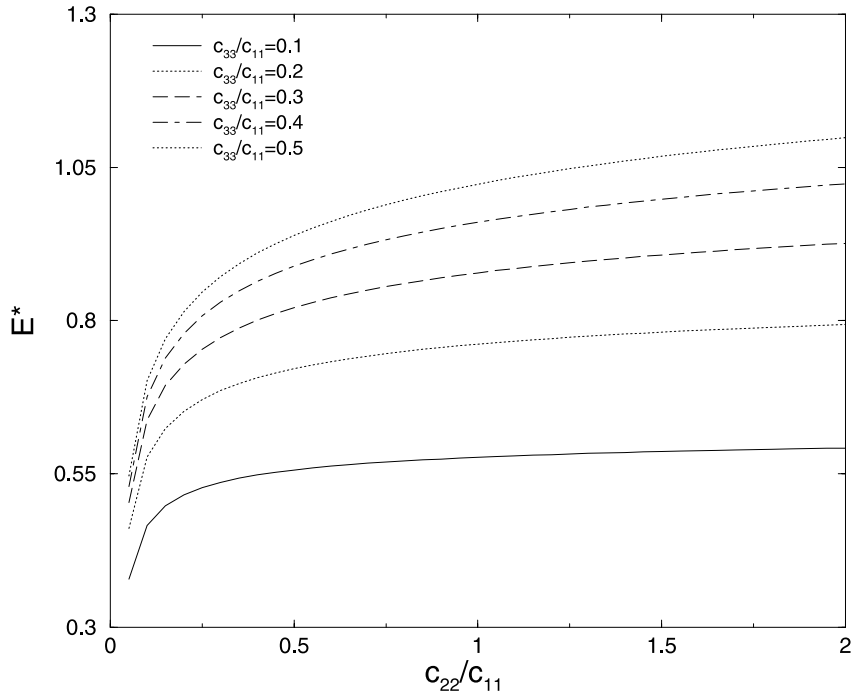

Fig. 3. Effects of material anisotropy on the effective modulus.

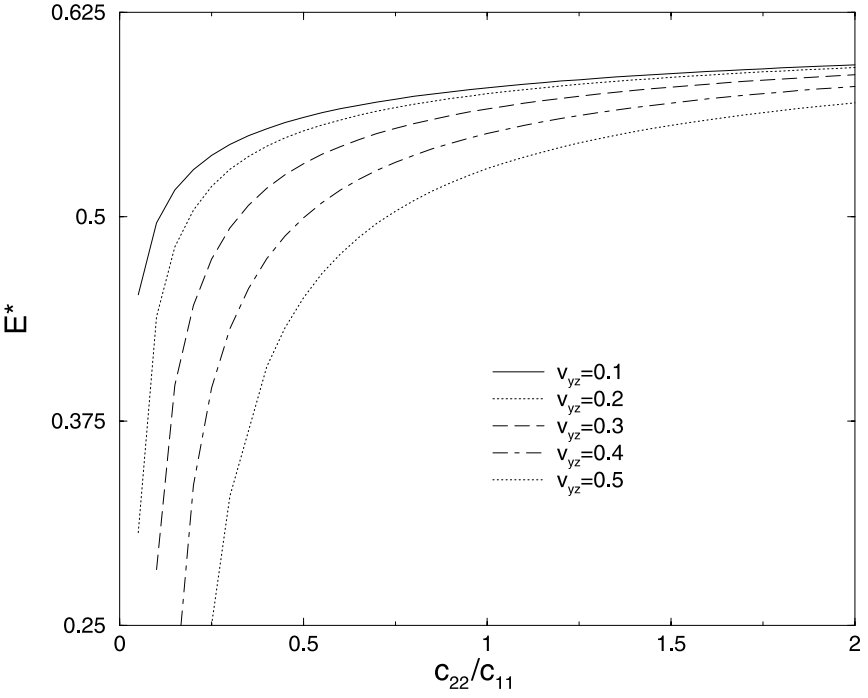

Fig. 4. Effects of the Poisson ratio on the effective modulus.

$$\sigma_{yz} = -S\frac{[K_7 f_2(\beta_1,\theta_1) + K_8 f_2(\beta_2,\theta_2)]}{\sqrt{r\pi}}, \tag{48}$$

where $f_1(\beta_i,\theta_i)$ and $f_2(\beta_i,\theta_i)$, $i = 0, 1, 2$ are known functions, and θ_i, β_i, $i = 0, 1, 2$ are known parameters given in Appendix D.

For $c_{33} = (\sqrt{c_{11}c_{22}} - c_{12})/2$, the singular field is

$$\sigma_y = S\frac{[\overline{K}_3 f_1(\beta_0,\theta_0) - \overline{K}_4 a_1 f_1(\beta_0,\theta_0) - \overline{K}_4 a_2 \frac{\partial}{\partial\theta} f_1(\beta_0,\theta_0)]}{\sqrt{r\pi}}, \tag{49}$$

$$\sigma_z = S\frac{[-\overline{K}_6 a_1 f_1(\beta_0,\theta_0) - \overline{K}_6 a_2 \frac{\partial}{\partial\theta} f_1(\beta_0,\theta_0)]}{\sqrt{r\pi}}, \tag{50}$$

$$\sigma_{yz} = -S\frac{[\overline{K}_7 f_2(\beta_0,\theta_0) - \overline{K}_8 a_1 f_2(\beta_0,\theta_0) - \overline{K}_8 a_2 \frac{\partial}{\partial\theta} f_2(\beta_0,\theta_0)]}{\sqrt{r\pi}}, \tag{51}$$

where $a_1 = \sin^2\theta$, $a_2 = \sin\theta\cos\theta$.

For $c_{33} > (\sqrt{c_{11}c_{22}} - c_{12})/2$, the singular field is

$$\sigma_y = S\frac{\left[\overline{\overline{K}}_3 \overline{\overline{f}}_1(\theta_3,\theta_4) + \overline{\overline{K}}_4 \overline{\overline{f}}_2(\theta_3,\theta_4)\right]}{\sqrt{r\pi}}, \tag{52}$$

$$\sigma_z = S\frac{\left[\overline{\overline{K}}_5 \overline{\overline{f}}_1(\theta_3,\theta_4) + \overline{\overline{K}}_6 \overline{\overline{f}}_2(\theta_3,\theta_4)\right]}{\sqrt{r\pi}}, \tag{53}$$

$$\sigma_{yz} = -S\frac{\left[\overline{\overline{K}}_7 \overline{\overline{f}}_4(\theta_3,\theta_4) + \overline{\overline{K}}_8 \overline{\overline{f}}_3(\theta_3,\theta_4)\right]}{\sqrt{r\pi}}, \tag{54}$$

where $\overline{\overline{f}}_1(\theta_3,\theta_4)$, $\overline{\overline{f}}_2(\theta_3,\theta_4)$ are known functions, and θ_3, θ_4 are known parameters defined in Appendix D.

Fig. 5 shows the angular distribution of the normalized singular stress field $f = (\sqrt{r\pi}\sigma_B/S)\sigma$ with different angle θ around the tip of the actuator, where σ represents σ_r, σ_θ and $\sigma_{r\theta}$, respectively. In this figure, $c_{22}/c_{11} = 11.53$ and $c_{12}/c_{11} = 0.46$. $\xi = (\sqrt{c_{11}c_{22}} - c_{12})/2c_{33}$ is assumed to be 0.25, 1, 4, respectively, representing the three phases discussed before. As expected, the maximum shear stress always occurs at $\theta = 180°$, i.e. along the interface, the maximum $\sigma_{\theta\theta}$ occurs around $\theta = 40°$–$60°$ ahead of the actuator, while for σ_{rr}, the maximum is at about $\theta = 130°$–$150°$. The actuator material is PZT-4, which has the following properties:

$$c_{11}^{(a)} = 13.9\times10^{10}\ (\text{Pa}), \quad c_{12}^{(a)} = 6.78\times10^{10}\ (\text{Pa}), \quad c_{13}^{(a)} = 7.43\times10^{10}\ (\text{Pa}),$$
$$c_{33}^{(a)} = 11.5\times10^{10}\ (\text{Pa}), \quad c_{44}^{(a)} = 2.56\times10^{10}\ (\text{Pa}),$$
$$e_{31}^{(a)} = -5.2\ (\text{C/m}^2), \quad e_{33}^{(a)} = 15.1\ (\text{C/m}^2), \quad e_{15}^{(a)} = 12.7\ (\text{C/m}^2),$$
$$\varepsilon_{11}^{(a)} = 6.45\times10^{-9}\ (\text{C/V m}), \quad \varepsilon_{33}^{(a)} = 5.62\times10^{-9}\ (\text{C/V m}).$$

Fig. 6 shows the normalized SSSF $S^* = S/\sigma_B\sqrt{2\pi h}$ for $c_{12}/c_{22} = 0.040$ and $c_{33}/c_{22} = 0.044$ correspondingly, $q = 3.019$. It shows a significant effect of the material anisotropy c_{11}/c_{22} upon the singular

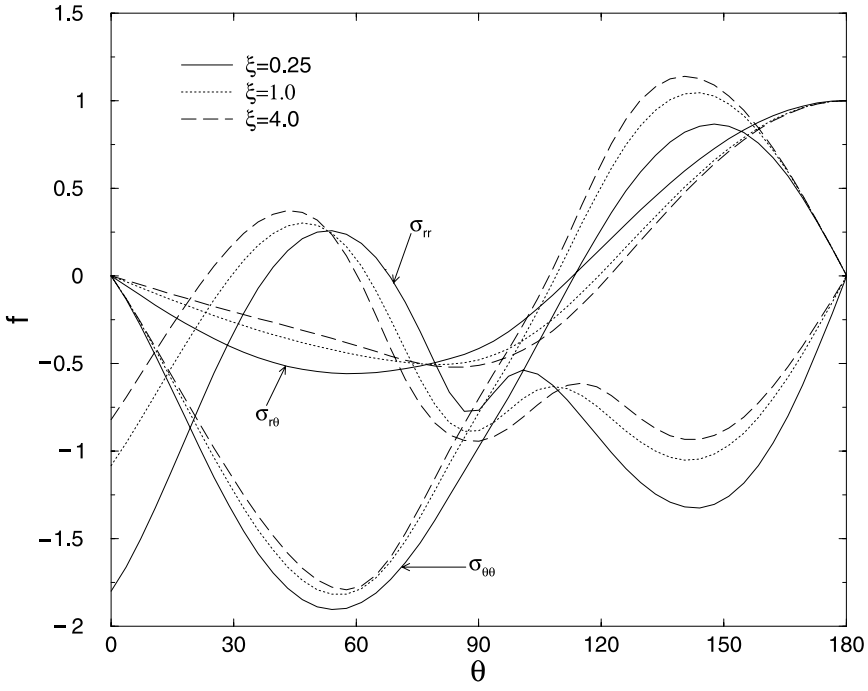

Fig. 5. Angular distribution of the normalized singular stress.

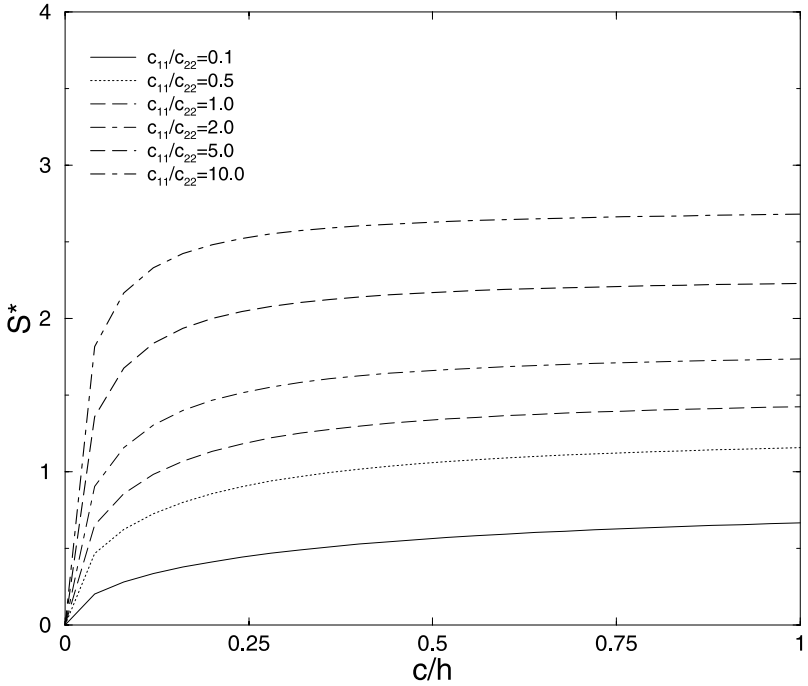

Fig. 6. Normalized SSSF.

stress field around the tip of the actuator. With the increase of the length of the actuator (c/h), the singular field will approach a steady state, as evidenced by the fact that S^* tends to a constant for large c/h.

5.3. Stress distribution along the interface

To validate the actuator model in determining the load transfer, interfacial stress predicted from the current model was compared with that from finite element analysis (ANSYS) using a PZT-4 actuator with finite thickness. Two different host media were considered:

Orthotropic medium:

$$c_{11}^{(1)} = 13.92 \times 10^{10}\ (\text{Pa}), \qquad c_{22}^{(1)} = 160.7 \times 10^{10}\ (\text{Pa}),$$
$$c_{33}^{(1)} = 7.07 \times 10^{10}\ (\text{Pa}), \qquad c_{12}^{(1)} = 6.44 \times 10^{10}\ (\text{Pa}).$$

Isotropic medium:

$$E^{(2)} = 5.4 \times 10^{11}\ (\text{Pa}), \qquad v^{(2)} = 0.3.$$

The orthotropic and isotropic media have the same effective modulus $\overline{E}$, which results in $q = 3.019$, as defined in Eq. (13). Our analytical model predicts that interfacial stress uniquely depends on q in considering the effect of the material properties. The comparison of $\overline{\tau} = \tau/\sigma_B$ resulting from different models in Fig. 7 for the case where $\alpha = 10$ confirmed this result. It is very interesting to mention that FEM results from orthotropic and isotropic media give very close interfacial stress distributions. The discrepancy

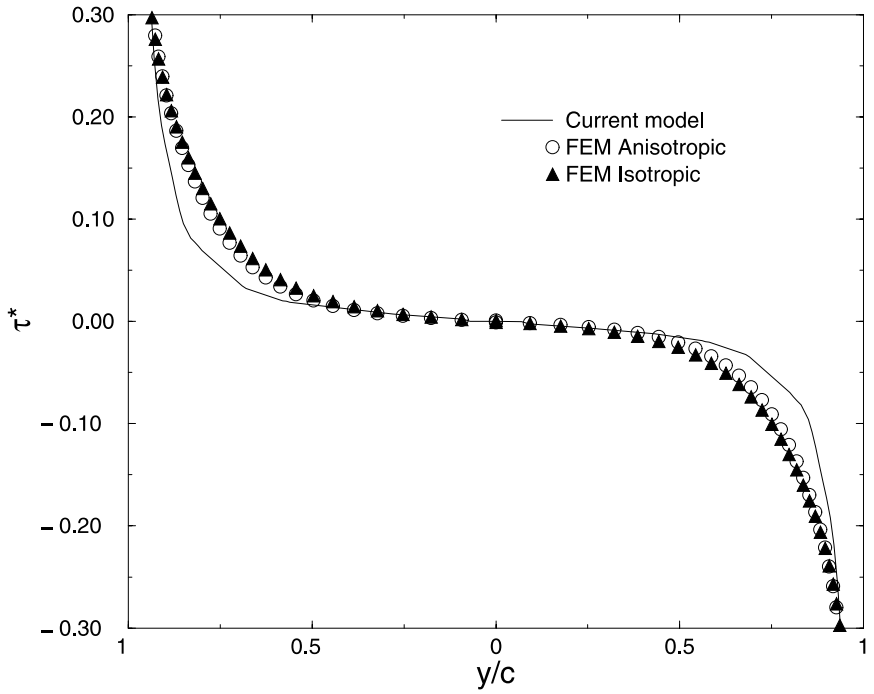

Fig. 7. Distribution of the interfacial shear stress.

between the analytical prediction and the FEM results may be caused by the one-dimensional assumption of the actuator.

5.4. Axial stress in debonded actuator

For the general case of central debonding, the debonded part will not experience interfacial shear stress. However, its effect on the load transfer will not disappear. In this case, the debonded region will affect the structure by applying a compressive (tensile) stress to the remaining parts of the actuator. Fig. 8 shows the normalized compressive axial stress $\sigma^* = |\sigma_d|/\sigma_B$, in the debonded part of the actuator for the case considered in Fig. 2. A significant effect of the anisotropic property of the host medium is observed.

5.5. Stress distribution in host medium

Fig. 9 shows the normalized stress distribution $\sigma_y^* = \sigma_y/\sigma_B$ in the host medium for $\alpha = 10$, $c_{22}/c_{11} = 11.53$, $c_{12}/c_{11} = 0.46$ and $c_{33}/c_{11} = 0.51$. σ_y was found highly localized in an area near the tip of the actuator. Fig. 10 shows the corresponding results for $\sigma_{yz}^* = \sigma_{yz}/\sigma_B$. For $z = 0.5h$ and $1.0h$, σ_{yz} undergoes a very sharp reduction around the tip of the actuator before it goes back to its 'normal' value. To further consider this issue, detailed FEM analysis was conducted, which did predict the same phenomenon. The numerical results for $z = 0.5h$ is compared with the corresponding analytical solution in Fig. 11. A good agreement can be observed. This phenomenon had also been observed in other material combinations.

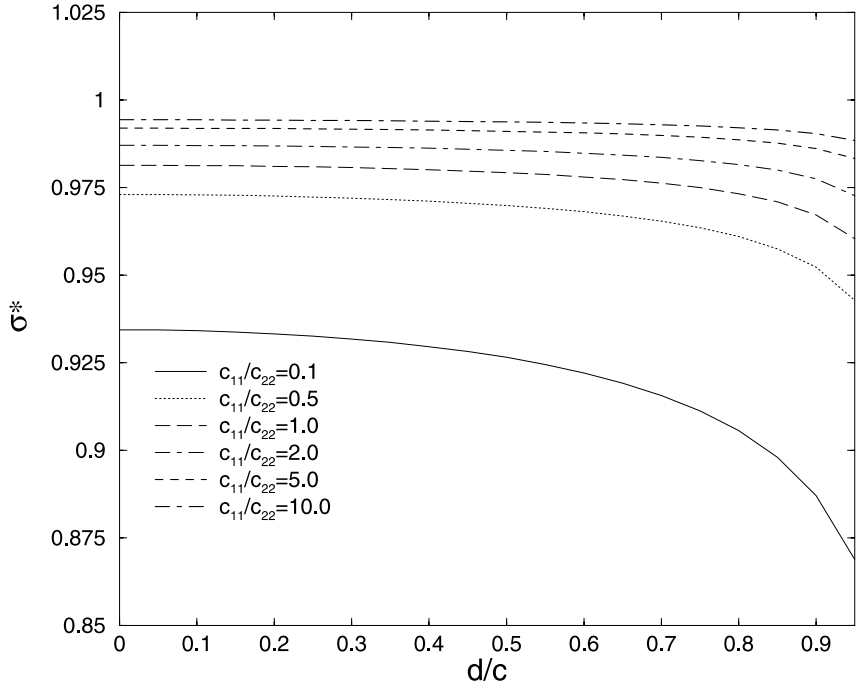

Fig. 8. The axial stress in a debonded actuator.

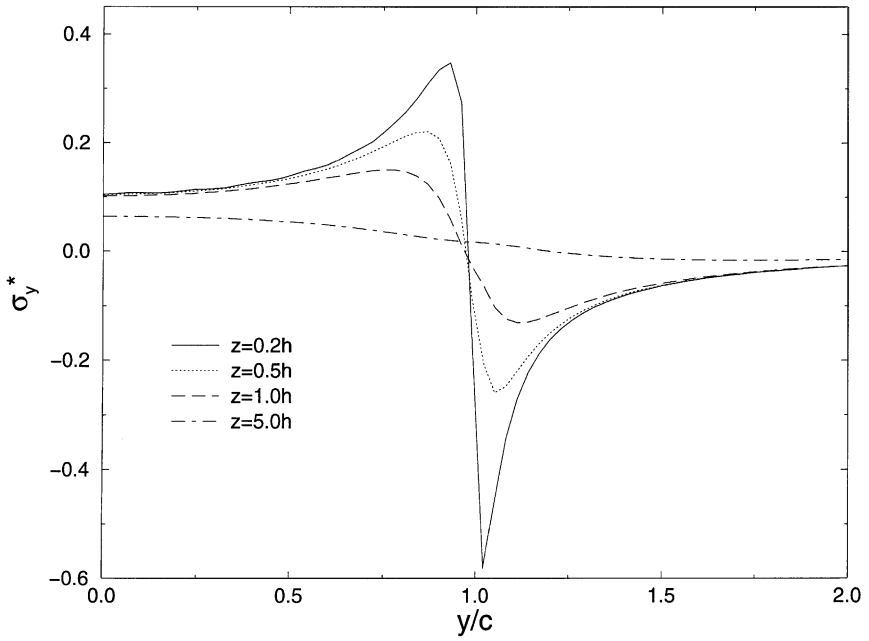

Fig. 9. Normal stress distribution in the host medium.

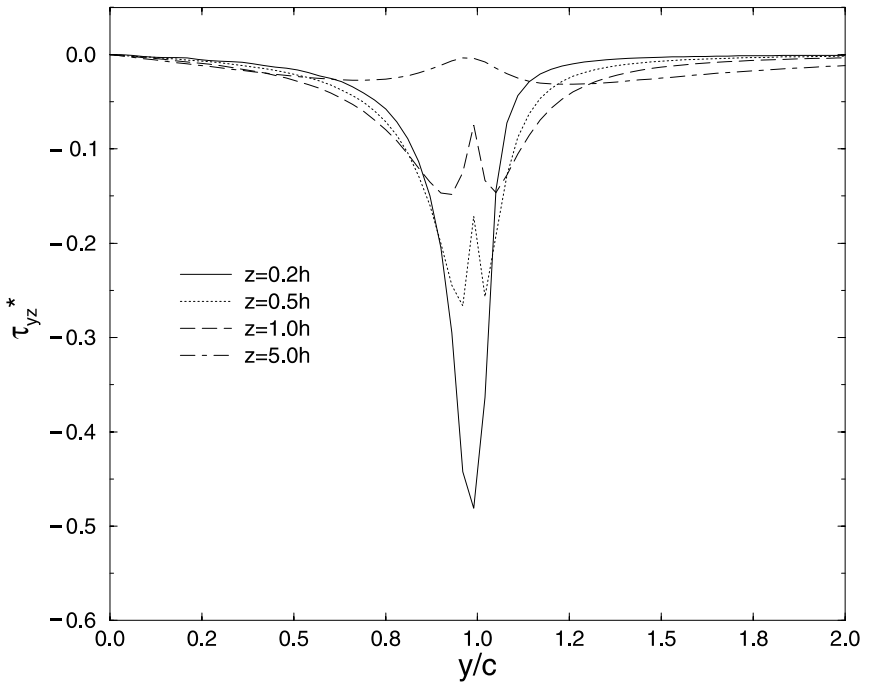

Fig. 10. Shear stress distribution in the host medium.

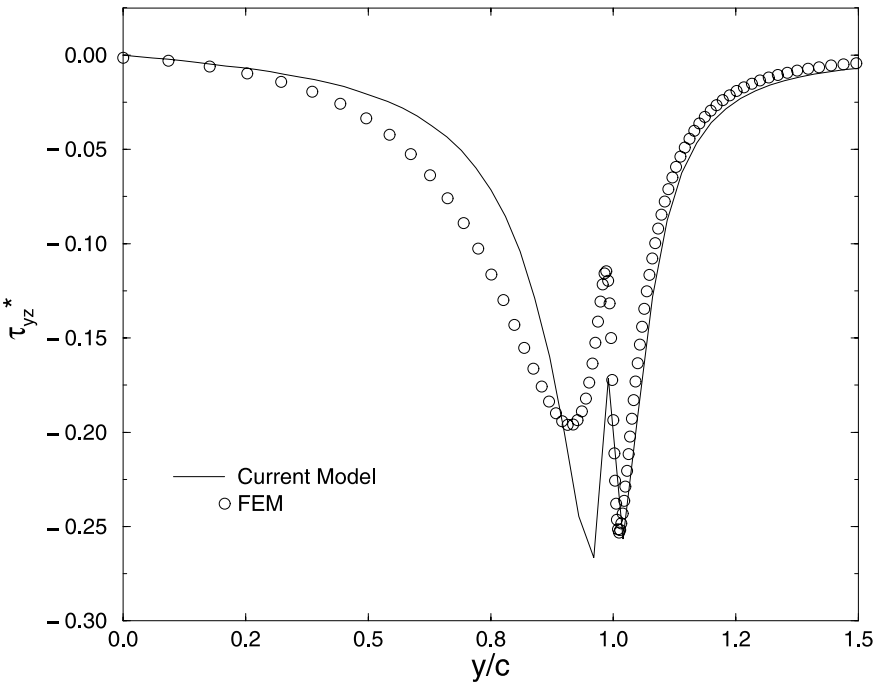

Fig. 11. Comparison of the analytical shear stress distribution with FEM results.

6. Concluding remarks

A general analytical solution is provided to the coupled electromechanical behavior of a piezoelectric actuator bonded to an orthotropic elastic medium under plane electric loading. The analysis is based on the use of a piezoelectric line model of the actuator and the solution of the resulting singular integral equations. The results show that the load transfer between the actuator and the host medium is governed by the effective moduli of the actuator and the host material.

The validity of the present model has been demonstrated by application to specific examples and comparison with the corresponding results obtained from finite element analyses. Furthermore, the effect of interfacial debonding on the load transfer are examined and discussed.

Acknowledgements

This work was supported by the Natural Sciences and Engineering Research Council of Canada.

Appendix A. Effective material constants

The mechanical and electrical properties of piezoceramic materials can be described by

$$\{\sigma\} = [c]\{\epsilon\} - [e]\{E\}, \qquad \{D\} = [e]\{\epsilon\} + [\varepsilon]\{E\},$$

where

$$\epsilon_{ij} = \tfrac{1}{2}(u_{i,j} + u_{j,i}), \qquad E_i = -V_{,i}.$$

In these equations, $\{\sigma\}$ and $\{\epsilon\}$ are the stress and the strain fields, $\{D\}$, $\{E\}$ and V represent the electric displacement, the electric field intensity and the potential, respectively. $[c]$ is a matrix containing the elastic stiffness parameters for a constant electric potential, $[e]$ represents a tensor containing the piezoelectric constants, and $[\varepsilon]$ represents the dielectric constants for zero strains.

According to the electroelastic line actuator model, $\sigma_z = 0$ and $\varepsilon_x = 0$. The effective material constants of the actuator can then be determined as

$$E_a = c_{11} - \frac{c_{13}^2}{c_{33}} \quad \text{plane strain},$$
$$e_a = e_{13} - e_{33}\frac{c_{13}}{c_{33}} \quad \text{plane strain},$$
$$\varepsilon_a = \varepsilon_{33} + \frac{e_{33}^2}{c_{33}} \quad \text{plane strain},$$

where the direction of polarization is designated as being the z axis.

Appendix B. Basic solution for an orthotropic medium

If the halfspace shown in Fig. 1 is an orthotropic medium whose principal elastic axes (in the two-dimensional case) are parallel to the y and z axes, respectively, the constitutive equation is as follows:

$$\begin{Bmatrix} \sigma_y \\ \sigma_z \\ \sigma_{yz} \end{Bmatrix} = \begin{bmatrix} c_{11} & c_{12} & 0 \\ c_{12} & c_{22} & 0 \\ 0 & 0 & c_{33} \end{bmatrix} \begin{Bmatrix} \varepsilon_y \\ \varepsilon_z \\ \varepsilon_{yz} \end{Bmatrix}.$$

Using the strain–displacement relation and substituting the constitutive relation into the equilibrium equations give

$$c_{11}\frac{\partial^2 v}{\partial^2 y} + c_{22}\frac{\partial^2 v}{\partial^2 z} + (c_{12} + c_{33})\frac{\partial^2 w}{\partial y \partial z} = 0,$$

$$c_{33}\frac{\partial^2 w}{\partial^2 y} + c_{22}\frac{\partial^2 w}{\partial^2 z} + (c_{12} + c_{33})\frac{\partial^2 v}{\partial y \partial z} = 0,$$

where w and v represent the displacement components along the z and y directions. Applying Fourier transform with respect to y defined by

$$\overline{v}(s,z) = \int_{-\infty}^{\infty} v(y,z)\,\mathrm{e}^{\mathrm{i}sy}\,\mathrm{d}y, \qquad \overline{w}(s,z) = \int_{-\infty}^{\infty} w(y,z)\,\mathrm{e}^{\mathrm{i}sy}\,\mathrm{d}y,$$

the equilibrium equations in the Fourier transform domain can be expressed as

$$c_{33}\frac{\partial^2 \overline{v}}{\partial^2 z} - c_{11}s^2\overline{v} - \mathrm{i}s(c_{12} + c_{33})\frac{\partial \overline{w}}{\partial z} = 0,$$

$$c_{22}\frac{\partial^2 \overline{w}}{\partial^2 z} - c_{33}s^2\overline{w} - \mathrm{i}s(c_{12} + c_{33})\frac{\partial \overline{v}}{\partial z} = 0.$$

From these equations, the two unknown functions $\overline{v}(s,z)$ and $\overline{w}(s,z)$ can be obtained, which are given in Eqs. (5) and (6).

Appendix C. General solution and stress field

The coefficients used in Eqs. (18)–(29) and (46)–(54) are given by

$$K_3=\frac{c_{11}K_1+c_{12}K_9\beta_1}{K_{11}},\quad K_4=\frac{c_{11}K_2+c_{12}K_{10}\beta_2}{K_{11}},\quad K_5=\frac{c_{12}K_1+c_{22}K_9\beta_1}{K_{11}},$$

$$K_6=\frac{c_{12}K_2+c_{22}K_{10}\beta_2}{K_{11}},\quad K_7=\frac{\beta_1}{\beta_1-\beta_2},\quad K_8=\frac{-\beta_2}{\beta_1-\beta_2},\quad K_9=\frac{\beta_1K_1K_2}{c_{33}(c_{12}+c_{33})},$$

$$K_{10}=\frac{-\beta_2K_1K_2}{c_{33}(c_{12}+c_{33})},\quad K_{11}=\frac{(\beta_1-\beta_2)K_1K_2}{(c_{12}+c_{33})},\quad \overline{K}_3=-\frac{c_{33}[(c_{12}\beta_0^2+c_{11})\overline{K}_1-2c_{22}\overline{K}_2\beta_0^2]}{\beta_0\overline{K}_2^2},$$

$$\overline{K}_4=\frac{c_{33}(c_{12}\beta_0^2+c_{11})}{\beta_0\overline{K}_2},\quad \overline{K}_5=0,\quad \overline{K}_6=-\frac{1}{\beta_0},\quad \overline{K}_7=1,\quad \overline{K}_8=-1,$$

$$\overline{\overline{K}}_3=\frac{c_{33}[c_{12}(\beta_3^2-\beta_4^2)\overline{\overline{K}}_1-2\beta_3\beta_4c_{12}\overline{\overline{K}}_2+c_{11}\overline{\overline{K}}_1]}{\overline{\overline{K}}_9(c_{12}+c_{33})},$$

$$\overline{\overline{K}}_4=\frac{c_{33}[c_{12}(\beta_3^2-\beta_4^2)\overline{\overline{K}}_2+2\beta_3\beta_4c_{12}\overline{\overline{K}}_1+c_{11}\overline{\overline{K}}_1]}{\overline{\overline{K}}_9(c_{12}+c_{33})},\quad \overline{\overline{K}}_5=0,\quad \overline{\overline{K}}_6=-\frac{1}{\beta_4},\quad \overline{\overline{K}}_7=1,\quad \overline{\overline{K}}_8=-\frac{\beta_3}{\beta_4},$$

$$\overline{\overline{K}}_9=\frac{-\beta_4(\overline{\overline{K}}_1^2+\overline{\overline{K}}_2^2)}{c_{12}+c_{33}}.$$

The functions of $F_{1j}(\phi_i,\theta_i)$, $F_{2j}(\phi_i,\theta_i)$, $F_{3j}(\phi_3,\theta_3,\phi_4,\theta_4)$, $F_{4j}(\phi_3,\theta_3,\phi_4,\theta_4)$, $F_{5j}(\phi_3,\theta_3,\phi_4,\theta_4)$ and $F_{6j}(\phi_3,\theta_3,\phi_4,\theta_4)$ in the local stress expressions (21)–(29) are

$$F_{1j}(\phi_i,\theta_i)=c^{j+1}\frac{\cos(\phi_ij-\theta_i/2)}{\Delta_i},\quad i=0,1,2,$$

$$F_{2j}(\phi_i,\theta_i)=c^{j+1}\frac{\sin(\phi_ij-\theta_i/2)}{\Delta_i}\operatorname{sgn}(y),\quad i=0,1,2,$$

$$F_{3j}=\frac{1}{2}c^{j+1}\left[\frac{\cos(\phi_3j-\theta_3/2)}{\Delta_3}+\frac{\cos(\phi_4j-\theta_4/2)}{\Delta_4}\right],$$

$$F_{4j}=-\frac{1}{2}c^{j+1}\left[\frac{\sin(\phi_3j-\theta_3/2)}{\Delta_3}\operatorname{sgn}(\beta_4z+y)+\frac{\sin(\phi_4j-\theta_4/2)}{\Delta_4}\operatorname{sgn}(\beta_4z-y)\right],$$

$$F_{5j}=\frac{1}{2}c^{j+1}\left[\frac{\cos(\phi_3j-\theta_3/2)}{\Delta_3}-\frac{\cos(\phi_4j-\theta_4/2)}{\Delta_4}\right],$$

$$F_{6j}=-\frac{1}{2}c^{j+1}\left[\frac{\sin(\phi_3j-\theta_3/2)}{\Delta_3}\operatorname{sgn}(\beta_4z+y)-\frac{\sin(\phi_4j-\theta_4/2)}{\Delta_4}\operatorname{sgn}(\beta_4z-y)\right],$$

where

$$\theta_0 = -\mathrm{arctg}\left(\frac{2|\beta_0 z||y|}{|\beta_0 z|^2 - |y|^2 + c^2}\right), \quad \phi_0 = -\mathrm{arctg}\left(\frac{R_0\sin(\theta_0/2) + |y|}{R_0\sin(\theta_0/2) + |\beta_0 z|}\right),$$

$$\theta_1 = -\mathrm{arctg}\left(\frac{2|\beta_1 z||y|}{|\beta_1 z|^2 - |y|^2 + c^2}\right), \quad \theta_2 = -\mathrm{arctg}\left(\frac{2|\beta_2 z||y|}{|\beta_2 z|^2 - |y|^2 + c^2}\right),$$

$$\theta_3 = -\mathrm{arctg}\left(\frac{2|\beta_4 z + y||\beta_3 z|}{|\beta_3 z|^2 - |\beta_4 z + y|^2 + c^2}\right), \quad \theta_4 = -\mathrm{arctg}\left(\frac{2|\beta_4 z - y||\beta_3 z|}{|\beta_3 z|^2 - |\beta_4 z - y|^2 + c^2}\right),$$

$$\phi_1 = -\mathrm{arctg}\left(\frac{R_1\sin(\theta_1/2) + |y|}{R_1\sin(\theta_1/2) + |\beta_1 z|}\right), \quad \phi_2 = -\mathrm{arctg}\left(\frac{R_2\sin(\theta_2/2) + |y|}{R_2\sin(\theta_2/2) + |\beta_2 z|}\right),$$

$$\phi_3 = -\mathrm{arctg}\left(\frac{R_3\sin(\theta_3/2) + |\beta_4 z + y|}{R_3\sin(\theta_3/2) + |Az|}\right), \quad \phi_4 = -\mathrm{arctg}\left(\frac{R_4\sin(\theta_4/2) + |\beta_4 z - y|}{R_4\sin(\theta_4/2) + |\beta_3 z|}\right),$$

$$R_0 = \sqrt[4]{\left(\beta_0^2 z^2 - y^2 + c^2\right)^2 + 4\beta_0^2 y^2 z^2}, \quad R_1 = \sqrt[4]{\left(\beta_1^2 z^2 - y^2 + c^2\right)^2 + 4\beta_1^2 y^2 z^2},$$

$$R_2 = \sqrt[4]{\left(\beta_2^2 z^2 - y^2 + c^2\right)^2 + 4\beta_2^2 y^2 z^2}, \quad R_3 = \sqrt[4]{\left(\beta_3^2 z^2 - (\beta_4 z + y)^2 + c^2\right)^2 + 4\beta_3^2(\beta_4 z + y)^2 z^2},$$

$$R_4 = \sqrt[4]{\left(\beta_3^2 z^2 - (\beta_4 z - y)^2 + c^2\right)^2 + 4\beta_3^2(\beta_4 z - y)^2 z^2},$$

$$\Delta_0 = R_0\left[\left(R_0\cos(\theta_0/2) + \beta_0^2 z^2\right)^2 + \left(R_0\sin(\theta_0/2) + y^2\right)^2\right]^{j/2},$$

$$\Delta_1 = R_1\left[\left(R_1\cos(\theta_1/2) + \beta_1^2 z^2\right)^2 + \left(R_1\sin(\theta_1/2) + y^2\right)^2\right]^{j/2},$$

$$\Delta_2 = R_2\left[\left(R_2\cos(\theta_2/2) + \beta_2^2 z^2\right)^2 + \left(R_2\sin(\theta_2/2) + y^2\right)^2\right]^{j/2},$$

$$\Delta_3 = R_3\left[\left(R_3\cos(\theta_3/2) + \beta_3^2 z^2\right)^2 + \left(R_3\sin(\theta_3/2) + (\beta_4 z + y)^2\right)^2\right]^{j/2},$$

$$\Delta_4 = R_4\left[\left(R_4\cos(\theta_4/2) + \beta_3^2 z^2\right)^2 + \left(R_4\sin(\theta_4/2) + (\beta_4 z - y)^2\right)^2\right]^{j/2}.$$

Appendix D. Singular stress field

The functions of $f_1(\beta_i, \theta_i), \overline{\overline{f}}_1(\theta_3, \theta_4), \overline{\overline{f}}_2(\theta_3, \theta_4), \overline{\overline{f}}_3(\theta_3, \theta_4), \overline{\overline{f}}_4(\theta_3, \theta_4)$ in the angular distribution field expressions (46)–(54) are

$$f_1(\beta_i, \theta_i) = \frac{\sin(|\theta_i|/2)}{\sqrt[4]{\cos(\theta)^2 + \beta_i^2\sin(\theta)^2}},$$

$$f_2(\beta_i, \theta_i) = \frac{\cos(|\theta_i|/2)}{\sqrt[4]{\cos(\theta)^2 + \beta_i^2\sin(\theta)^2}}, \quad i = 0, 1, 2,$$

$$\overline{\overline{f}}_1(\theta_3, \theta_4) = \tfrac{1}{2}[f_3(\theta_3) + f_3(\theta_4)], \overline{\overline{f}}_2(\theta_3, \theta_4) = \tfrac{1}{2}[f_4(\theta_4) - f_4(\theta_3)],$$

$$\overline{\overline{f}}_3(\theta_3, \theta_4) = \tfrac{1}{2}[f_4(\theta_3) + f_4(\theta_4)], \overline{\overline{f}}_4(\theta_3, \theta_4) = \tfrac{1}{2}[f_3(\theta_3) - f_3(\theta_4)],$$

where

$$\theta_0 = -\mathrm{arctg}\left[-\frac{\beta_0 \sin(\theta)}{\cos(\theta)}\right], \quad \theta_1 = -\mathrm{arctg}\left[-\frac{\beta_1 \sin(\theta)}{\cos(\theta)}\right], \quad \theta_2 = -\mathrm{arctg}\left[-\frac{\beta_2 \sin(\theta)}{\cos(\theta)}\right],$$

$$\theta_3 = -\mathrm{arctg}\left[-\frac{\beta_3 \sin(\theta)}{\beta_4 \sin(\theta) + \cos(\theta)}\right], \quad \theta_4 = -\mathrm{arctg}\left[-\frac{\beta_3 \sin(\theta)}{\beta_4 \sin(\theta) - \cos(\theta)}\right],$$

$$f_3(\theta_i) = \frac{\sin(|\theta_i|/2)}{\sqrt[4]{\beta_3^2 \sin(\theta)^2 + (\beta_4 \cos(\theta) + \sin(\theta))^2}},$$

$$f_4(\theta_i) = \frac{\cos(|\theta_i|/2)}{\sqrt[4]{\beta_3^2 \sin(\theta)^2 + (\beta_4 \cos(\theta) + \sin(\theta))^2}}, \quad i = 3, 4.$$

References

Ashley, S., 1995. Smart skis and other adaptive structures. Mechanical Engineering, November, 76–81.

Banks, H.T., Smith, R.C., 1995. The modeling of piezoceramic patch interactions with shells plates and beams. Quaterly of Applied Mathematics LIII, 353–381.

Crawley, E.F., Anderson, E.H., 1990. Detailed models of piezoelectric actuation of beams. Journal of Intelligent Material Systems and Strctures 1, 4–25.

Crawley, E.F., Luis, J., 1987. Use of piezoelectric actuators as elements of intelligent structures. AIAA Journal 25, 1373–1385.

Dimitriadis, E.K., Fuller, C.R., Rogers, C.A., 1991. Piezoelectric actuators for distributed noise and vibration excitation of thin plates. Journal of Vibration and Acoustics 13, 100–107.

Gandhi, M.V., Thompson, B.S., 1992. Smart Materials and Structures. Chapman & Hall, London.

Ha, S.K., Kerlers, C., Chang, F.K., 1992. Finite element analysis of composite structures containing distributed piezoelectric sensors and actuators. AIAA Journal 30, 772–780.

Han, J.-H., Lee, I., 1998. Analysis of composite plates with piezoelectric actuators for vibration control using layerwise displacement theory. Composites, Part B 29, 519–672.

Im, S., Atluri, S.N., 1989. Effects of a piezo-actuator on a finite deformation beam subjected to general loading. AIAA Journal 27, 1801–1807.

Lim, Y.-H., Gopinathan, S.V., Varadan, V.V., Varadan, V.K., 1999. Finite element simulation of smart structures using an optimal output feedback controller for vibration and noise control. Smart Materials and Structures 8, 324–337.

Lin, M.W., Rogers, C.A., 1993a. Modeling of the actuation mechanism in a beam structure with induced strain actuators. Proceedings of AIAA/ASCE/ASME/ASC 34th Structures, Structural Dynamics and Materials Conference, Part VI, La Jolla, CA, April 19–22. AIAA, Washington, DC, pp. 3608–3617.

Lin, M.W., Rogers, C.A., 1993b. Actuation response of a beam structure with induced strain actuators. Adaptive Structures and Material Systems AD 35, 129–139.

Mitchell, J.A., Reddy, J.N., 1995. A study of embedded piezoelectric layers in composite cylinders. ASME Journal of Applied Mechanics 62, 166–173.

Muskhelishvili, N.I., 1953. Some Basic Problems of the Mathematical Theory of Elasticity. Noordhoff, Groningen.

Reddy, J.N., 1997. Mechanics of Laminated Composite Plates, Theory and Analysis. CRC Press, Boca Raton, FL.

Reddy, J.N., 1999. On laminated composite plates with integrated sensors and actuators. Engineering Structures 21, 568–593.

Tauchert, T.R., 1992. Piezothermoelastic behavior of a laminated plate. Journal of Thermal Stresses 15, 25–37.

Tzou, H.S., Tseng, C.I., 1991. Distributed vibration control and identification of coupled elastic/piezoelectric systems. Mechanical Systems and Signal Processing 5, 215–231.

Tzou, H.S., Ye, R., 1994. Piezothermoelasticity and precision control of piezoelectric systems: theory and finite element analysis. Journal of Vibration and Acoustics 116, 489–495.

Varadan, V.K., Wu, Z., Bao, X.-Q., Varadan, V.V., 1993. Light weight robot using piezoelectric motor, sensor and actuator. Adaptive Structures and Material Systems AD 35, 141–148.

Wang, X.D., Meguid, S.A., 2000. On the electroelastic behavior of a thin piezoelectric actuator attached to an infinite host structrue. International Journal of Solids and Structures 37, 3231–3251.

Wang, B.-T., Rogers, C.A., 1991. Laminate plate theory for spatially distributed induced strain actuators. Journal of Composite Materials 25, 433–452.